Title

Metabolic characterization of human IDH mutant and wild type gliomas using simultaneous pH- and oxygen-sensitive molecular MRI

Permalink

Journal

ISSN

Authors

Yao, Jingwen
Chakhoyan, Ararat
Nathanson, David A
et al.

Publication Date

DOI

Peer reviewed

Neuro-Oncology

Metabolic characterization of human IDH mutant and wild type gliomas using simultaneous pH- and oxygen-sensitive molecular MRI

Jingwen Yao, Ararat Chakhoyan, David A. Nathanson, William H. Yong, Noriko Salamon, Catalina Raymond, Sergey Mareninov, Albert Lai, Phioanh L. Nghiemphu, Robert M. Prins, Whitney B. Pope, Richard G. Everson, Linda M. Liau, Timothy F. Cloughesy, and Benjamin M. Ellingson

UCLA Brain Tumor Imaging Laboratory, Center for Computer Vision and Imaging Biomarkers, University of California Los Angeles, Los Angeles, California (J.Y., A.C., C.R., B.M.E.); Department of Radiological Sciences, David Geffen School of Medicine, University of California Los Angeles, Los Angeles, California (J.Y., A.C., N.S., C.R., W.B.P., B.M.E.); Department of Bioengineering, Henry Samueli School of Engineering and Applied Science, University of California Los Angeles, Los Angeles, California (J.Y., B.M.E.); UCLA Neuro-Oncology Program, University of California Los Angeles, Los Angeles, California (A.L., P.L.N., T.F.C., B.M.E.); Department of Neurosurgery, David Geffen School of Medicine, University of California Los Angeles, Los Angeles, California (R.M.P., R.G.E., L.M.L.); Department of Neurology, David Geffen School of Medicine, University of California Los Angeles, Los Angeles, California (A.L., P.L.N., T.F.C.); Department of Molecular and Medical Pharmacology, David Geffen School of Medicine, University of California Los Angeles, Los Angeles, California (D.A.N.); Department of Pathology, David Geffen School of Medicine, University of California Los Angeles, Los Angeles, California (W.H.Y., S.M.)

Corresponding Author: Benjamin M. Ellingson, Ph.D. Director, UCLA Brain Tumor Imaging Laboratory (BTIL) Associate Professor of Radiology, Biomedical Physics, Psychiatry, and Bioengineering Departments of Radiological Sciences and Psychiatry David Geffen School of Medicine University of California, Los Angeles 924 Westwood Blvd., Suite 615, Los Angeles, CA 90024 (bellingson@mednet.ucla.edu).

Abstract

Background. Isocitrate dehydrogenase 1 (IDH1) mutant gliomas are thought to have distinct metabolic characteristics, including a blunted response to hypoxia and lower glycolytic flux. We hypothesized that non-invasive quantification of abnormal metabolic behavior in human IDH1 mutant gliomas could be performed using a new pH- and oxygen-sensitive molecular MRI technique.

Methods. Simultaneous pH- and oxygen-sensitive MRI was obtained at 3T using amine CEST-SAGE-EPI. The pH-dependent measure of the magnetization transfer ratio asymmetry (MTR_{asym}) at 3 ppm and oxygen-sensitive measure of R_2' were quantified in 90 patients with gliomas. Additionally, stereotactic, image-guided biopsies were performed in 20 patients for a total of 52 samples. The association between imaging measurements and hypoxia-inducible factor 1 alpha (HIF1α) expression was identified using Pearson correlation analysis.

Results. IDH1 mutant gliomas exhibited significantly lower MTR_{asym} at 3 ppm, R_2', and $MTR_{asym}xR_2'$ ($P = 0.007$, $P = 0.003$, and $P = 0.001$, respectively). $MTR_{asym}xR_2'$ could identify IDH1 mutant gliomas with a high sensitivity (81.0%) and specificity (81.3%). HIF1α was positively correlated with MTR_{asym} at 3 ppm, R_2' and $MTR_{asym}xR_2'$ in IDH1 wild type ($r = 0.610$, $P = 0.003$; $r = 0.667$, $P = 0.008$; $r = 0.635$, $P = 0.006$), but only $MTR_{asym}xR_2'$ in IDH1 mutant gliomas ($r = 0.727$, $P = 0.039$).

Conclusions. IDH1 mutant gliomas have distinct metabolic and microenvironment characteristics compared with wild type gliomas. An imaging biomarker combining tumor acidity and hypoxia ($MTR_{asym}xR_2'$) can differentiate IDH1 mutation status and is correlated with tumor acidity and hypoxia.

Key Points

1. A combined MRI biomarker for acidity and hypoxia can differentiate IDH1 mutation status.

2. HIF1α expression is correlated with acidity and hypoxia in IDH1 wild type, but not mutant gliomas.

Importance of the Study

The current study builds on the current body of literature around IDH1 mutant glioma metabolism by using a unique, clinically available pH- and oxygen-sensitive molecular imaging technique to explore tumor acidity and hypoxia in IDH1 mutant and wild type human gliomas. Results suggest IDH1 mutations are associated with lower tumor acidity and lower vascular hypoxia. The observed differences within the tumor microenvironment likely reflect metabolic differences, which is further supported by our observation of differential sensitivity of imaging measures of tumor acidity and hypoxia to HIF1α expression between IDH1 mutant and wild type gliomas. This study provides additional evidence that IDH1 mutant gliomas have distinct metabolic characteristics and suggests pH- and oxygen-sensitive MRI may be a valuable clinical imaging biomarker for identifying altered metabolic characteristics or for quantifying response to metabolically targeted therapies.

Mutations in NADP+ dependent isocitrate dehydrogenase (IDH) genes,[1] IDH1 (mutations at residue R132), or IDH2 (mutations at residue R172) occur in a majority of World Health Organization (WHO) grades II and III gliomas and secondary glioblastoma (>80%).[2] IDH mutant gliomas in adult patients are often non-enhancing,[3,4] occur frequently in the frontal lobe,[4,5] and have better clinical outcome compared with IDH wild type gliomas,[1,6] suggesting that there are unique physiological characteristics of IDH mutant gliomas that may make them particularly vulnerable to specific therapies.

IDH1 and IDH2 are primarily localized in the cytosol and mitochondria, respectively, and catalyze the oxidative decarboxylation of isocitrate to generate alpha-ketoglutarate (αKG) and produce NADPH (Fig. 1). The mutations of IDH1[R132] or IDH2[R172] result in a loss of affinity to isocitrate along with a new enzymatic ability to reduce αKG to the D-enantiomeric isoform of 2-hydroxyglutarate (D-2-HG), coupled with the oxidation of NADPH to NADP+.[1,7] The oncometabolite, 2-HG, is thought to contribute to malignant transformation of glioma through multiple pathways, including increase in reactive oxygen species (ROS) level, disturbance of the NADPH/NADP+ balance, and competitive inhibition of αKG-dependent enzymes.[8]

Despite the known signaling pathways involved in IDH1 mutant gliomas, the downstream impact of IDH1 mutations on energy metabolism remains controversial. Prolyl-hydroxylase domain (PHD) is an αKG-dependent enzyme responsible for the oxygen-dependent degradation of hypoxia-inducible factor 1 alpha (HIF1α) (Fig. 1). HIF1α is a key factor that mediates the cell energy production under hypoxia, shifting glucose metabolism from oxidative phosphorylation to less efficient glycolytic pathway,[9] leading to the accumulation of lactic acid and a reduction in extracellular pH. Additionally,

HIF1α activates angiogenesis-related signaling and plays part in tumor cell self-renewal and proliferation.[10] Oncometabolite 2-HG generated from mutation in IDH1 was first reported to stabilize HIF1α through inhibition of PHD.[11,12] However, more contemporary studies have offered contradictory findings, suggesting that 2-HG may activate PHD, promoting HIF1α degradation and downregulating HIF1α target genes.[13,14] This appears to agree with a separate study showing decreased mRNA expression of HIF1α and downstream effects in patient IDH1 mutant tumors.[15] Additionally, a study by Grassian et al[16] observed increased oxidative tricarboxylic acid metabolism, decreased reductive glutamine metabolism, and reduced tumor growth rates in IDH1 mutant glioma cells under hypoxic conditions, suggesting IDH1 mutant gliomas prefer a more oxygenated microenvironment for continual proliferation. Based on these studies, we hypothesized IDH1 mutant gliomas would be both less acidic and less hypoxic compared with IDH1 wild type gliomas.

The current study builds on the current body of literature around IDH1 mutant glioma metabolism by using a unique, clinically available pH- and oxygen-sensitive molecular imaging technique termed amine chemical exchange saturation transfer spin-and-gradient-echo echoplanar imaging (CEST-SAGE-EPI)[17] to explore tumor acidity and hypoxia in IDH1 mutant and wild type human gliomas. CEST-SAGE-EPI provides pH sensitivity through quantification of the chemical exchange between amine protons in bulk water, which has been shown to be pH dependent.[18] The inherently elevated concentration of glutamine within tumors[19–21] further increases the available proton exchange, resulting in a higher CEST signal at 3.0 ppm.[22,23] Additionally, the reversible transverse relaxation rate, R_2', which has been shown to be proportional
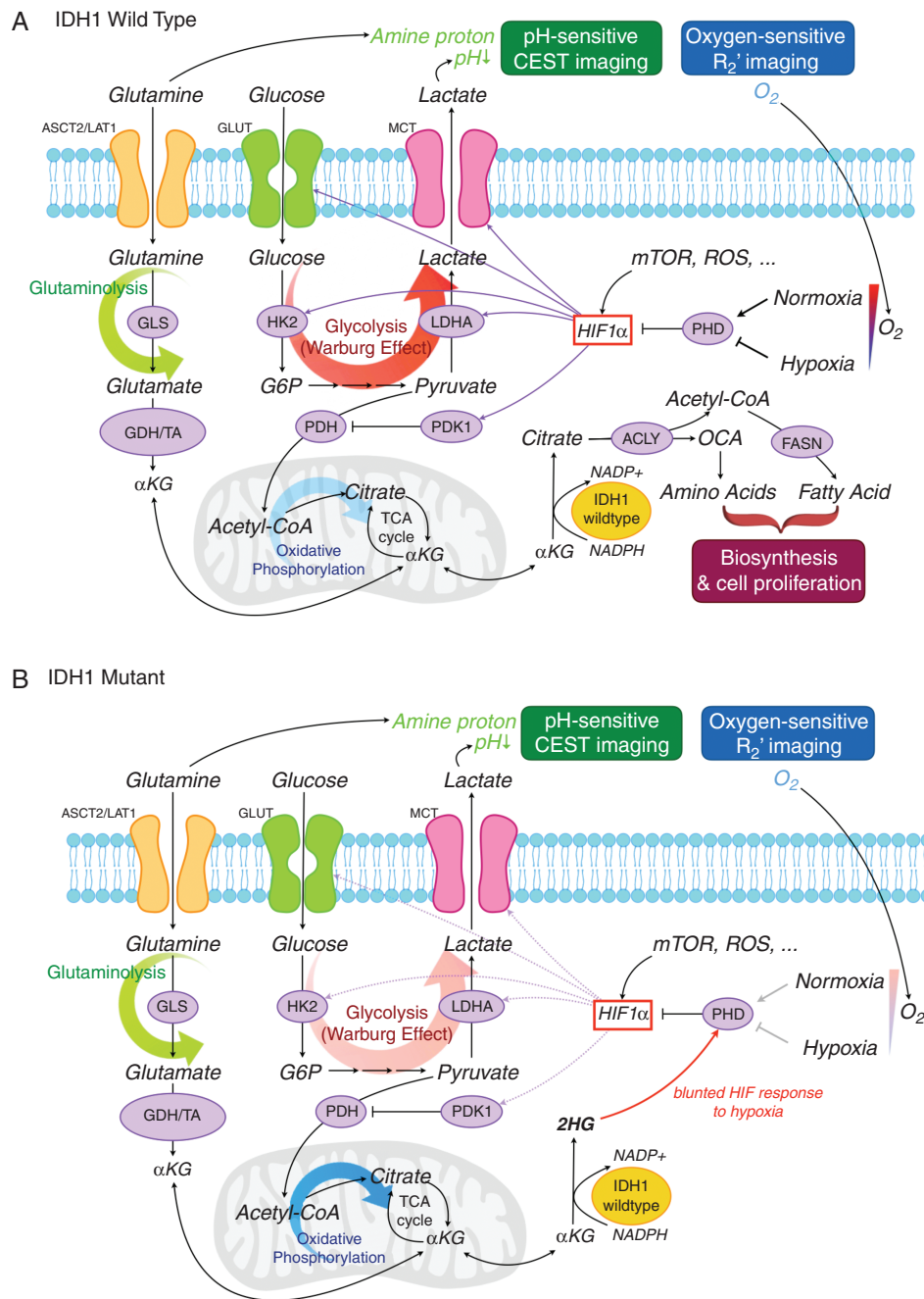
Fig. 1 Metabolic differences between IDH1 wild type and IDH1 mutant gliomas. (A) IDH1 wild type gliomas, like other malignant tumors, are characterized by a high level of glycolysis (Warburg effect). (B) Unlike wild type gliomas, IDH mutant gliomas produce the oncometabolite 2-HG, which activates PHD, leading to blunted HIF1α response to hypoxia, and lower levels of HIF1α. This lower HIF1α may shift the metabolism to oxidative phosphorylation, reducing glycolytic activity, and subsequently reducing tumor acidity by reduction of lactic acid. ASCT2/LAT1: glutamine transporters; GLUT: glucose transporters; MCT: monocarboxylate transporters; GLS: glutaminase; GDH: glutamate dehydrogenase; TA: transaminase; aKG: alpha-ketoglutarate; HK2: hexokinase-2; G6P: glucose-6-phosphate; LDHA: lactic dehydrogenase A; PDH: pyruvate dehydrogenase; PDK1: pyruvate dehydrogenase kinase 1; acetyl-CoA: acetyl coenzyme A; TCA cycle: tricarboxylic acid cycle; mTOR: mammalian target of rapamycin; ACLY: ATP citrate lyase; OCA: obeticholic acid; FASN: fatty acid synthase.

to oxygen extraction fraction and tumor oxygenation,[24–28] can be simultaneously quantified using the multi-echo readout obtained using CEST-SAGE-EPI. In order to further characterize tumor acidity and hypoxia in IDH1 mutant and wild type gliomas, we also performed MRI-guided biopsy and immunohistochemistry to explore the link between CEST-SAGE-EPI measurements and both HIF1α and Ki67 expression.

Materials and Methods

Patients

A total of 90 histologically proven glioma patients were included in this retrospective study: 21 patients with WHO grade II, 29 patients with WHO grade III, and 40 patients with WHO grade IV. Of these 90 patients, 60 patients were scanned either prior to radiation therapy and/or chemotherapy including temozolomide (N = 56), with (N = 16) or without (N = 40) prior tumor resection surgery or had been off treatment for more than 2 years (N = 4). The other 30 patients were either on active treatment or recently off treatment at the time of MRI scanning. Detailed patient characteristics are further outlined in Table 1 and Fig. 2. All patients provided informed written consent to have advanced imaging and medical information included in our institutional review board–approved research database or provided informed written consent to have image-guided biopsies for research purposes. All patients had CEST-SAGE-EPI or CEST-EPI (single echo) and routine MRI scanning between April 2015 and June 2018, with good image quality as well as IDH1 mutation status available from resected or biopsied tissue. IDH1 mutation status was determined by genomic sequencing analysis using polymerase chain reaction and/or immunohistochemistry (IHC) as described previously.[4] Loss of 1p/19q was assessed with fluorescence in situ hybridization.[29]

Amine CEST-SAGE-EPI and Anatomic MRI Acquisition

Simultaneous acquisition of pH-weighted amine CEST contrast and oxygen-sensitive R_2' mapping was performed using the CEST-SAGE-EPI pulse sequence, as previously described.[17] This sequence consists of a CEST saturation pulse train of three (3x) 100-ms Gaussian pulses with peak amplitude B_1 = 6 μT and a spin-and-gradient-echo (SAGE)-EPI readout consisting of 2 gradient echoes with echo times (TEs) = 14.0 and 34.1 ms, one asymmetric spin-echo with TE = 58.0 ms, and one spin-echo with TE = 92.4 ms. Additional acquisition parameters include a repetition time (TR) >10 000 ms, field of view = 217 × 240 mm, matrix size = 116 × 128, slice thickness = 4.0 mm with no interslice gap, partial Fourier encoding = 6/8, GRAPPA (generalized autocalibrating partially parallel acquisition) = 3, and bandwidth = 1628 Hz/pixel. A total of 29 z-spectral points was acquired at offset frequency from −3.5 ppm to −2.5 ppm; from −0.3 ppm to +0.3 ppm; and from +2.5 ppm to +3.5 ppm, all with respect to the water proton resonance frequency. An additional reference (S_0) scan was obtained with 4 averages using identical parameters and no saturation pulses. All MRIs were acquired on 3T MR scanners (Prisma or Skyra, Siemens Healthcare). Of the 90 scans, 35 were performed using single-echo pH-weighted CEST-EPI sequence[23] with TE = 27 ms and no oxygen-sensitive information. The total acquisition time for CEST-SAGE-EPI was 7 minutes and 30 seconds benchmarked on a 3T Siemens Prisma MR scanner (Software Versions VE11A-C). In addition to CEST scan prior to contrast administration, all patients received the anatomic images according to the standardized brain tumor imaging protocol.[30]

CEST-SAGE-EPI Data Post-Processing

All CEST-SAGE-EPI and CEST-EPI images were motion corrected using an affine transformation (*mcflirt*; Functional Magnetic Resonance Imaging of the Brain Software Library) and B_0 correction via a z-spectra based k-means clustering and Lorentzian fitting algorithm.[31] Following motion and B_0 correction, the integral of width of 0.4 ppm was quantified around both the −3.0 and +3.0 ppm (−3.2 to −2.8 ppm and +2.8 to +3.2 ppm, respectively) spectral points. These data points were combined with the S_0 image to calculate the asymmetry in the magnetization transfer ratio asymmetry (MTR_{asym}) at 3.0 ppm, a measure related to pH,[23] as defined using equation: $MTR_{asym}(3.0\ ppm) = S(-3.0\ ppm)/S_0 - S(+3.0\ ppm)/S_0$, where $S(\omega)$ is the amount of bulk water signal available after the saturation pulse with offset frequency ω and S_0 is the signal available without application of radiofrequency saturation. For CEST-SAGE-EPI data, the average MTR_{asym} at 3.0 ppm was calculated by averaging the first (TE = 14.0 ms) and second (TE = 34.1 ms) gradient echoes to increase the available signal-to-noise.
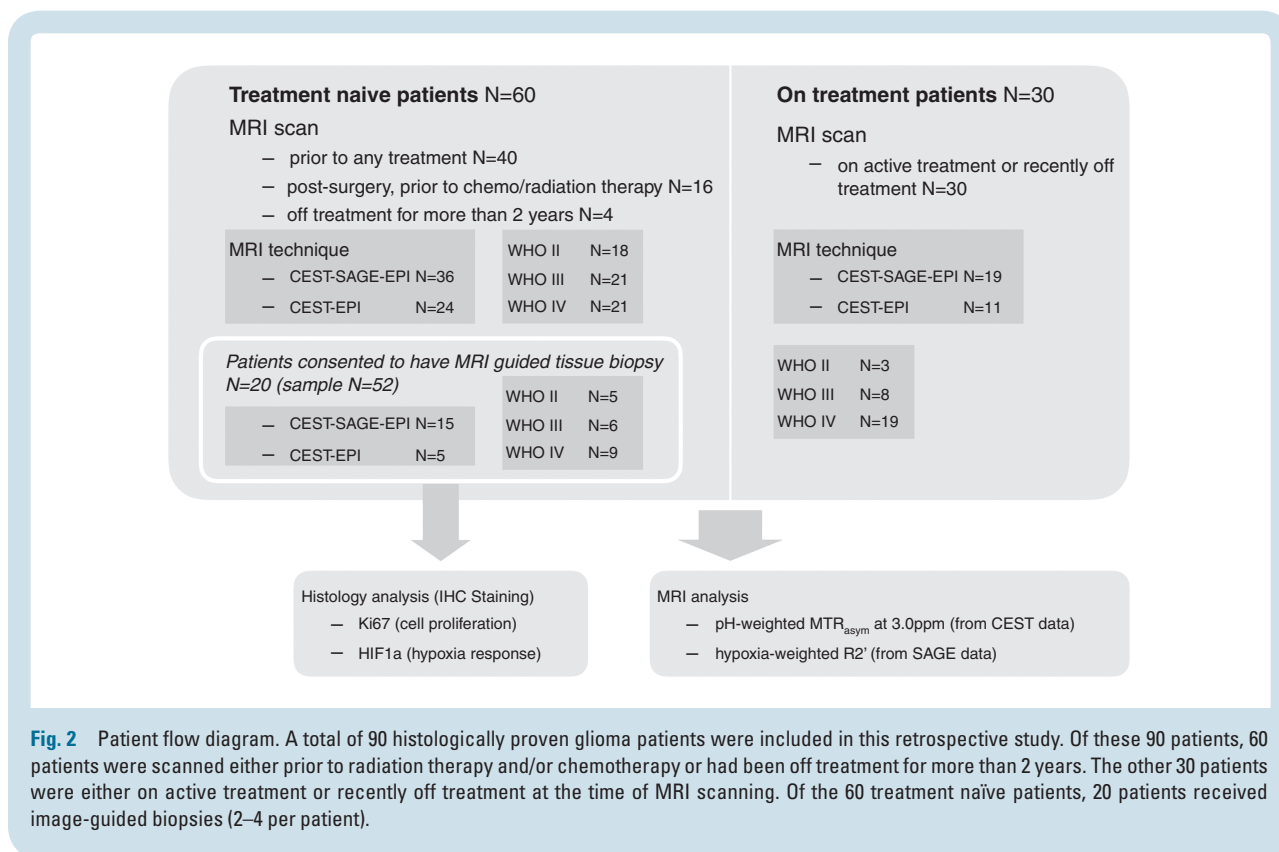
Estimates of transverse relaxation rates R_2, R_2^*, and $R_2' = R_2^* - R_2$, which is proportional to oxygen extraction, were obtained by solving a system of Bloch equations as detailed previously.[17] All post-processing was performed with MatLab (release 2017b, MathWorks). All resulting maps were registered to high-resolution post-contrast T1-weighted images for subsequent analyses.

Immunohistochemistry Staining of HIF1α and Ki67

Fifty-two tissue samples from 20 patients were acquired with MRI-guided tissue biopsy prior to surgical resection.

Table 1 Patient demographics

	All Patients	Grade II	Grade III	Grade IV
No. of patients (treatment naïve/on treatment)	90 (60/30)	21 (18/3)	29 (21/8)	40 (21/19)
Age median [range]	51.5 [15–90]	40 [22–90]	48 [15–70]	60 [19–81]
Sex male/female	58/32	8/13	18/11	32/8
IDH1 status wild type/mutant	52/38	2/19	12/17	38/2
1p/19q status in IDH1-mutant intact/codeleted/NA	21/12/5	9/9/1	13/3/1	0/0/2

Fig. 2 Patient flow diagram. A total of 90 histologically proven glioma patients were included in this retrospective study. Of these 90 patients, 60 patients were scanned either prior to radiation therapy and/or chemotherapy or had been off treatment for more than 2 years. The other 30 patients were either on active treatment or recently off treatment at the time of MRI scanning. Of the 60 treatment naïve patients, 20 patients received image-guided biopsies (2–4 per patient).

Two to 4 MRI targets (spheres with 5 mm diameter) were selected for each patient based on the MTR_{asym} at 3.0 ppm and R_2' images. Targets were placed in regions with high/low acidity and high/low hypoxia. Immunohistochemical analysis was performed on 5 μm formalin-fixed paraffin embedded tissue sections. Heat-induced antigen retrieval was accomplished with Antigen Decloaker buffer, pH 6.0 in a Decloaking Chamber at 95°C for 30 min (Biocare Medical). Tissue sections were then treated with 3% peroxide and with Background Sniper (Biocare Medical) to reduce nonspecific background staining. Primary antibodies for HIF1α (Sigma-Aldrich) were applied in a 1:200 dilution for 80 min followed by detection with the Mach 3 horseradish peroxidase (HRP) polymer detection system (Biocare Medical). Subsequent immunodetection was completed using HRP substrate Vector NovaRed (Vector Laboratories) and counterstained with hematoxylin. Primary antibodies for Ki67 (SP6, Sigma-Aldrich) were applied in a 1:100 dilution for 60 min followed by the same detection procedure. Tissue slides were scanned with digital slide scanner Aperio CS2 (Aperio Technologies). The positive cell percentage is calculated as the ratio of positive cell number and total cell number in a specific tissue section area, using positive cell detection algorithm with QuPath.[32]

Data Analysis and Statistics

Four mutually exclusive regions of interest (ROIs) were defined: (i) normal-appearing white matter (NAWM) contralateral to the tumor; (ii) contrast enhancing tumor (CE)

defined by T1-weighted digital subtraction[33]; (iii) regions of central necrosis defined by hypointensity on post-contrast T1-weighted images; and (iv) T2 hyperintense regions on T2-weighted fluid attenuated inversion recovery (FLAIR) images, excluding areas of necrosis and contrast enhancement. All ROIs except for NAWM were segmented using a semi-automated thresholding method.[33]

Median MTR_{asym} at 3.0 ppm (acidity), R_2' (hypoxia), and the product $MTR_{asym} \times R_2'$ (reflecting the degree of both acidity *and* hypoxia) within tumor ROI excluding necrosis (combined ROI of contrast-enhancing tumor [ii] and non-enhancing T_2 hyperintense tumor [iv]) were compared between IDH1 mutant and wild type gliomas, and 1p/19q codeletion status, using Student's *t*-test or Wilcoxon rank-sum test if one or both samples are not normally distributed as assessed by a Shapiro–Wilk parametric hypothesis test. Median MTR_{asym} at 3.0 ppm, R_2', and $MTR_{asym} \times R_2'$ within tumor ROI were also compared across WHO grades using one-way ANOVA. *P*-values less than 0.05 were considered statistically significant. All metrics were reported as mean ± standard deviation. Receiver operating characteristic (ROC) analysis was performed to assess the ability for MTR_{asym} at 3.0 ppm, R_2', and $MTR_{asym} \times R_2'$ to discriminate IDH1 status. Area under the curve (AUC), cutoff value, and prediction accuracy (percentage of cases predicted correctly) were reported. Lastly, the correlation between MTR_{asym} at 3.0 ppm, R_2', and $MTR_{asym} \times R_2'$ and quantitative IHC results were reported using Pearson's correlation coefficient, *r*, and corresponding *P*-value. All calculations and analysis were carried out using MatLab (release 2017b, MathWorks).

Results

In general, IDH1 mutant gliomas (Fig. 3A, C) had lower acidity and hypoxia compared with IDH1 wild type gliomas (Fig. 3B, D, E), even when controlling for tumor grade (Fig. 3A–D). Exceedingly high acidity and hypoxia were observed within contrast enhancing areas, particularly in IDH1 wild type glioblastomas (Fig. 3E). MTR_{asym} at 3 ppm, R_2' and $MTR_{asym}xR_2'$ were significantly different and increasing with increasing WHO grade (Supplementary Table 1; *ANOVA*; MTR_{asym} *P = 0.005*; R_2' *P = 0.005*, $MTR_{asym}xR_2'$ *P = 0.013*); however, these differences were not observed after controlling for IDH1 status.

Acidity and Hypoxia in Different Tissue Types

CE tumor, T_2 hyperintense FLAIR regions, and areas of central necrosis exhibited significantly higher acidity compared with NAWM, as measured by MTR_{asym} at 3 ppm on CEST-SAGE-EPI or CEST-EPI (Supplementary Fig. 1A; *P < 0.001*). This was true for both treatment naïve patients (Supplementary Fig. 1D; *N = 60*) and all patients, including patients previously treated with surgical resection with or without radiation and/or chemotherapy (*N = 90*). Areas of necrosis had the highest levels of acidity, followed by regions of CE, FLAIR hyperintense regions, and NAWM.

In the subset of patients who received CEST-SAGE-EPI for which R_2' was available (*N = 55*), T_2 hyperintense regions (5.67 ± 2.46 s^{-1}) exhibited significantly lower R_2' compared with NAWM (6.61 ± 1.35 s^{-1}, *P < 0.001*), while CE lesions and necrosis (15.20 ± 9.43 s^{-1}, 13.88 ± 9.49 s^{-1}) exhibited significantly higher R_2' compared with NAWM and T_2 hyperintense lesions (Supplementary Fig. 1B; *P < 0.001* for all comparisons). No difference in R_2' was observed between CE and necrotic regions (*P = 0.598*). These same trends were observed when examining treatment naïve patients exclusively (Supplementary Fig. 1E; *N = 36*).

The degree of both acidity and hypoxia, quantified by $MTR_{asym}xR_2'$, followed trends of similar MTR_{asym} at 3 ppm (Supplementary Fig. 1F). Necrosis and CE tumor had the highest $MTR_{asym}xR_2'$ and were not significantly different (*P = 0.143;* 6.92 ± 3.11 vs 4.30 ± 1.93), but were significantly different compared with both T_2 hyperintense regions (25.65 ± 15.68; *P < 0.001*) and NAWM (19.88 ± 8.17; *P < 0.001*). Similar trends were observed when considering only treatment naïve patients (Supplementary Fig. 1F; *N = 36*).

Acidity and Hypoxia in IDH1 Mutant and Wild Type Gliomas

Consistent with qualitative observations, MTR_{asym} at 3 ppm within T_2 hyperintense regions were significantly lower in IDH1 mutant compared with IDH1 wild type gliomas (Fig. 4A; 1.52% ± 0.39% vs 1.78% ± 0.47%, *P = 0.007*). This difference, however, was removed after excluding WHO IV glioblastomas (IDH1 mutant: 1.50% ± 0.40%; IDH1 wild type: 1.73% ± 0.51%, *P = 0.102*). R_2' was also significantly lower in IDH1 mutant compared with wild type gliomas (Fig. 4B; 4.95 ± 2.37 s^{-1} vs 6.87 ± 2.78 s^{-1}, *P = 0.003*), but not after excluding glioblastomas (*P = 0.080*). $MTR_{asym}xR_2'$, reflecting the degree of both acidity and hypoxia, were also significantly lower in IDH1 mutant compared with wild type gliomas (Fig. 4C; 5.91 ± 3.28 vs 8.48 ± 3.44, *P = 0.001*), even when examining lower grades exclusively (WHO II–III) (5.83 ± 3.32 vs 8.48 ± 3.44, *P = 0.023*). The same trends were observed when considering only treatment naïve patients.

ROC analysis suggested the best differentiation of treatment naïve IDH1 mutant from wild type gliomas was achieved using $MTR_{asym}xR_2'$ with a threshold of 6.58, which resulted in a sensitivity and specificity of 81.0% and 81.3%, respectively (Fig. 4D; *AUC = 0.86; P = 0.0002*). $MTR_{asym}xR_2'$ was also able to differentiate IDH1 mutation status when treated patients were included, albeit with slightly lower sensitivity (73.1%) and specificity (70.0%) (Fig. 4E; *AUC = 0.76, P = 0.0008*). Differentiation of IDH1 mutant from wild type gliomas using $MTR_{asym}xR_2'$ can be further visualized by plotting MTR_{asym} versus R_2' (Fig. 4F, G), where the cutoff value for best ROC performance defined by $MTR_{asym}xR_2' = 6.58$ is illustrated.

Acidity and Hypoxia in 1p/19q Codeleted and Intact IDH1 Mutant Gliomas

MTR_{asym} at 3.0 ppm was significantly lower in 1p/19q codeleted IDH1 mutant gliomas compared with 1p/19q intact gliomas (Fig. 4H; 1.29% ± 0.30% vs 1.61% ± 0.41%, *P = 0.024*). No significant difference in R_2' (Fig. 4I; 1p/19q codeleted; 4.54 ± 2.46 s^{-1}, 1p/19q intact; 4.48 ± 1.86 s^{-1}, *P = 0.926*) or in $MTR_{asym}xR_2'$ (1p/19q codeleted; 5.05 ± 2.86, 1p/19q intact; 5.37 ± 1.81, *P = 0.306*) were observed. These same characteristics were observed when only treatment naïve patients were considered (MTR_{asym}; *P = 0.035*, R_2'; *P = 0.649* and $MTR_{asym}xR_2'$; *P = 0.543*). Within only WHO II gliomas, lower MTR_{asym} was also associated with 1p/19q codeleted (*P = 0.027*; treatment naïve, *P = 0.016*), suggesting that this difference may originate from molecular features.

Correlation Between MRI Measures of Tumor Acidity and Hypoxia with IHC

To better understand the association between MRI measures of acidity and hypoxia and histological features of the tumor including HIF1α and Ki67 expression, we performed multiple image-guided biopsies in glioma patients from select regions with high or low MTR_{asym} at 3 ppm and R_2'. Figure 5 illustrates examples of MRI-based biopsy targets (red spheres in Fig. 5A, D, G) along with corresponding HIF1α (Fig. 5B, E, H) and Ki67 (Fig. 5C, F, I) expression within those areas (note all samples were counterstained with hematoxylin). Quantitative estimates of the proportion of cells with stain positivity demonstrated an interesting dichotomy between IDH1 mutant and wild type tumors (Fig. 6). Specifically, we observed a positive correlation between MTR_{asym} at 3 ppm and the proportion of HIF1α positive cells in IDH1 wild type (*r = 0.610, P = 0.003*) but not in
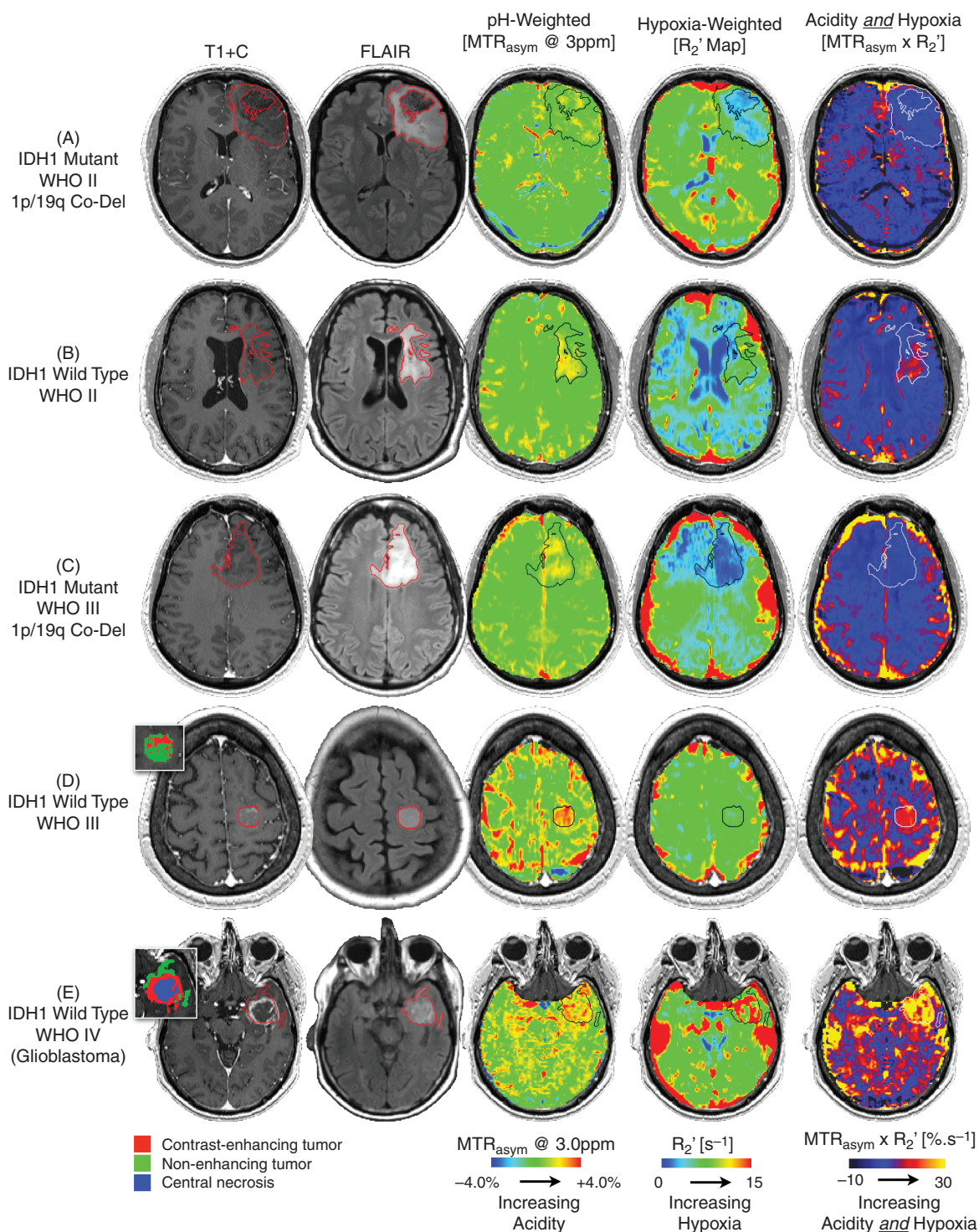
Fig. 3 pH- and oxygen-sensitive molecular MR images in representative glioma patients. (A) A 34-year-old female patient with a WHO grade II, IDH1 mutant, 1p/19q codeleted glioma with only slightly elevated acidity within T2 hyperintense regions on FLAIR (outlined in red), reduced oxygen extraction illustrated by decreased R_2' compared with normal tissue. (B) A 43-year-old male patient with a WHO grade II, IDH1 wild type glioma showing elevated acidity and hypoxia within T2 hyperintense regions. (C) A 43-year-old male patient with a WHO grade III, IDH1 mutant glioma showing small pockets of slightly elevated acidity and substantially lower R_2' compared with normal white matter. (D) A 60-year-old female patient with a WHO grade III, IDH1 wild type malignant glioma (anaplastic astrocytoma) illustrating an isolated, non-enhancing lesion with high acidity and oxygen extraction similar to surrounding white matter. (E) A 69-year-old male patient with a WHO grade IV, IDH1 wild type glioblastoma illustrating high levels of both tumor acidity and hypoxia.
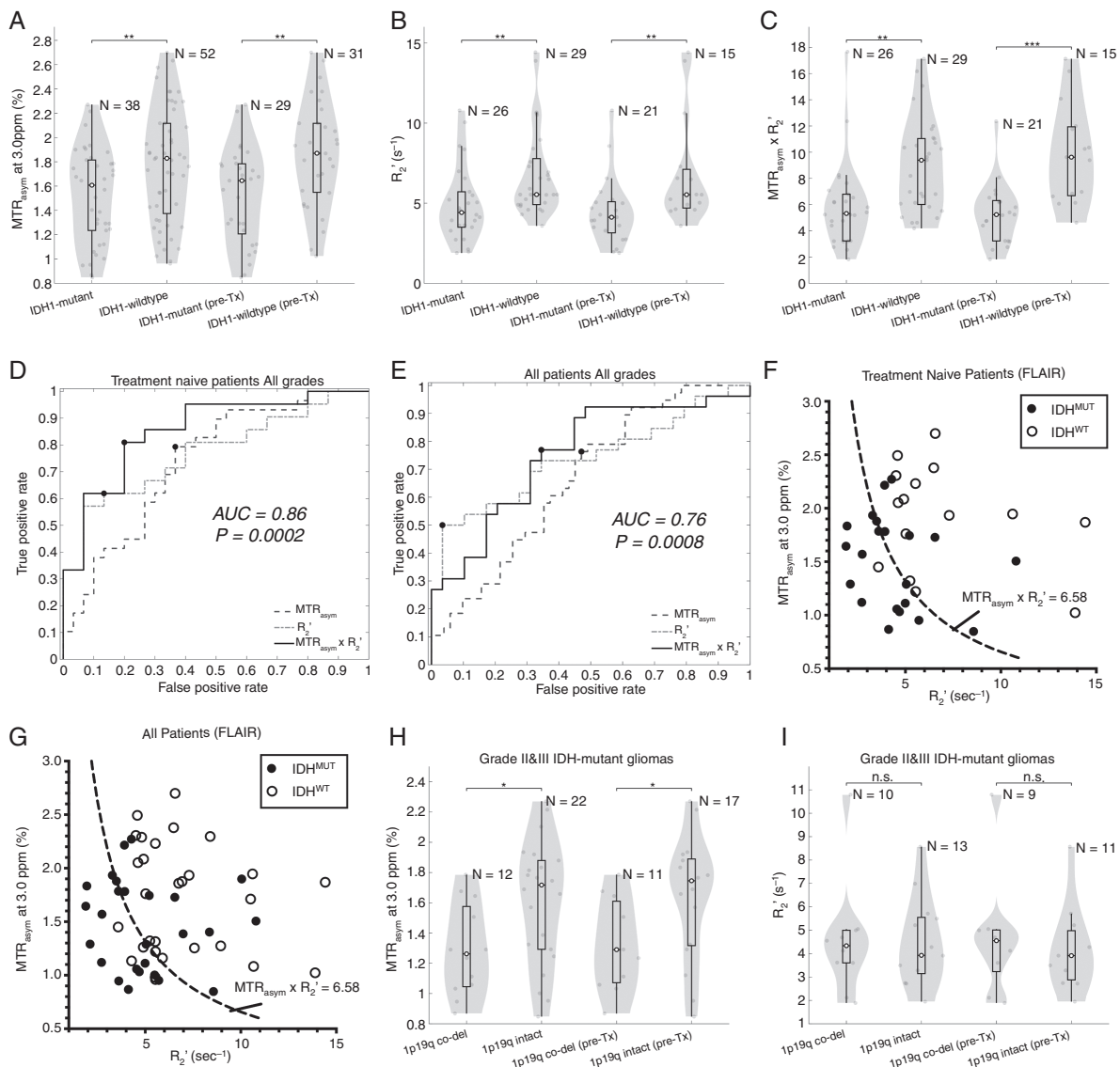
Fig. 4 Quantitative comparison of pH and hypoxia characteristics of IDH1 mutant and wild type gliomas. (A) Comparison of MTR_{asym}, (B) R_2', and (C) $MTR_{asym} \times R_2'$ measurements between IDH1 mutant and wild type gliomas in all patients (left panel) and in a subset of treatment naïve patients (right panel). IDH1 mutant gliomas exhibited less acidity (lower MTR_{asym} at 3 ppm) and less hypoxia (lower R_2') compared with IDH1 wild type gliomas in both all patients ($P < 0.01$, $P < 0.01$) and in untreated subgroup ($P < 0.01$, $P < 0.01$). The differentiation between IDH1 mutant and IDH1 wild type gliomas was further increased by using a single metric for tumor acidity *and* hypoxia, $MTR_{asym} \times R_2'$ in treatment naïve patients ($P < 0.01$) and all patients, including those on active therapy ($P < 0.001$). Black boxes reflect interquartile range with median of the distribution (circle). (D) ROC curves for MTR_{asym}, R_2', and $MTR_{asym} \times R_2'$ in treatment naïve patients including all grades, showing best area under the curve (AUC = 0.86, $P = 0.0002$) when using the degree of acidity and hypoxia ($MTR_{asym} \times R_2'$). (E) ROC curves for MTR_{asym}, R_2', and $MTR_{asym} \times R_2'$ in all evaluable patients including all grades, showing best area under the curve (AUC = 0.76, $P = 0.0008$) when using $MTR_{asym} \times R_2'$. (F) Plots illustrating combined pH- and hypoxia-weighted MR measurements in treatment naïve IDH1 mutant (solid black circles) and wild type gliomas (open circles) with best delineation at $MTR_{asym} \times R_2' = 6.58$ (dashed line). (G) Plots illustrating combined pH- and hypoxia-weighted MR measurements in all patients with IDH1 mutant (solid black circles) or wild type gliomas (open circles). (H) Comparison of acidity (MTR_{asym} at 3 ppm) between 1p/19q codeleted and intact, WHO grade II–III, IDH1 mutant gliomas showing lower acidity in 1p/19q codeleted tumors ($P < 0.05$). (I) Comparison of hypoxia (R_2') between 1p/19q codeleted and intact, WHO grade II-III, IDH1 mutant gliomas showing no difference between subtypes.

IDH1 mutant gliomas (Fig. 6A; *r = 0.080, P = 0.805*). A moderate correlation was also found between MTR_{asym} at 3 ppm and the proportion of Ki67 positive cells in IDH1 mutant (Fig. 6B; *r = 0.451, P = 0.027*), but not wild type gliomas (*r = 0.240, P = 0.273*), which may have been at least partly

due to necrotic tissue also having high MTR_{asym} at 3 ppm. R_2' was positively correlated with the proportion of HIF1α positive cells in IDH1 wild type (*r = 0.667, P = 0.008*), but not in IDH1 mutant gliomas (Fig. 6C; *r = 0.782, P = 0.198*). Similarly, a positive correlation was observed between
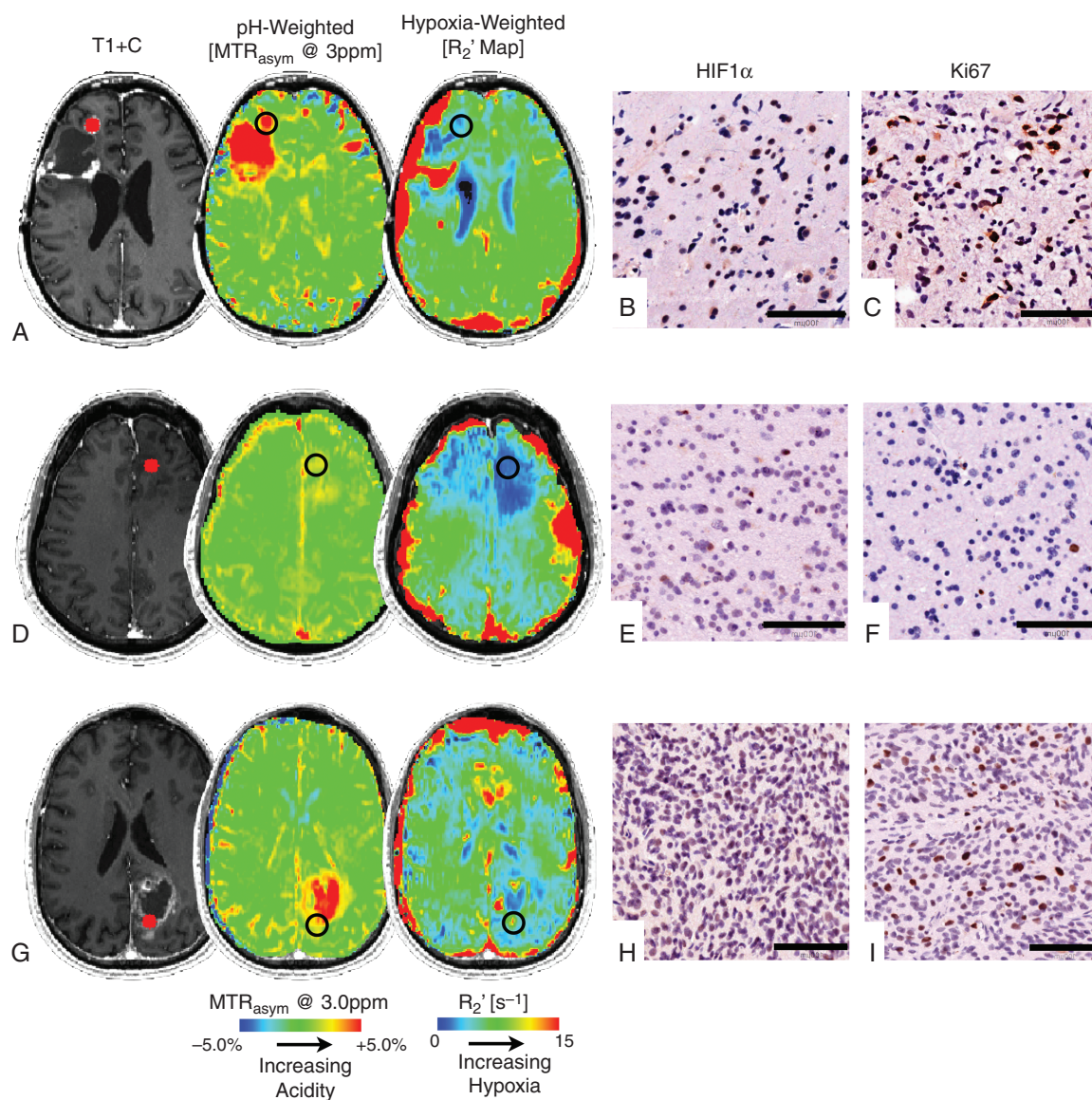
Fig. 5 MRI-guided biopsy targets and corresponding IHC staining for HIF1α and Ki67. (A) Post-contrast T1-weighted images (T1+C), pH-weighted images (MTR$_{asym}$ at 3 ppm), and hypoxia-weighted images (R$_2$') in an IDH1 mutant, recurrent glioblastoma patient with localized contrast enhancement, elevated acidity (high MTR$_{asym}$ at 3 ppm) and low hypoxia (R$_2$'). (B) HIF1α and (C) Ki67 stained slides of from a 5 mm radius biopsy sample taken from the MRI-guided biopsy target (red dot and black circles). (D) A WHO grade III, IDH1 mutant, 1p/19q codeleted recurrent malignant glioma with low acidity and low hypoxia, along with corresponding (E) HIF1α and (F) Ki67 stained slides from the MRI-guided target. (G) A newly diagnosed, IDH wild type glioblastoma patient with elevated acidity and hypoxia, along with corresponding (H) HIF1α and (I) Ki67 stained slides from the MRI-guided target. For both HIF1α and Ki67, cells negative for expression are blue (hematoxylin only), while positive cells are brown. IHC image scaling: 100 μm.

R$_2$' and the proportion of Ki67 positive cells in IDH1 wild type ($r = 0.513$, $P = 0.028$) but not in mutant gliomas (Fig. 6D; $r = 0.788$, $P = 0.165$). Measures of MTR$_{asym}$×R$_2$', thought to reflect the degree of both acidity and hypoxia, were positively correlated with the proportion of HIF1α positive cells in both IDH1 mutant ($r = 0.727$, $P = 0.039$) and wild type gliomas (Fig. 6E; $r = 0.635$, $P = 0.006$). However, MTR$_{asym}$×R$_2$' was only correlated with Ki67 in IDH1 wild type ($r = 0.601$, $P = 0.018$) and not IDH1 mutant gliomas (Fig. 6F; $r = 0.314$, $P = 0.673$).

Discussion

The current study demonstrates the potential of simultaneous pH- and oxygen-sensitive amine CEST-SAGE-EPI to provide important metabolic information about gliomas. Results suggest that the degree of tumor acidity and hypoxia, measured using a single measure of MTR$_{asym}$×R$_2$', may be a useful imaging biomarker for differentiating IDH1 and 1p/19q status in both treated and untreated gliomas,
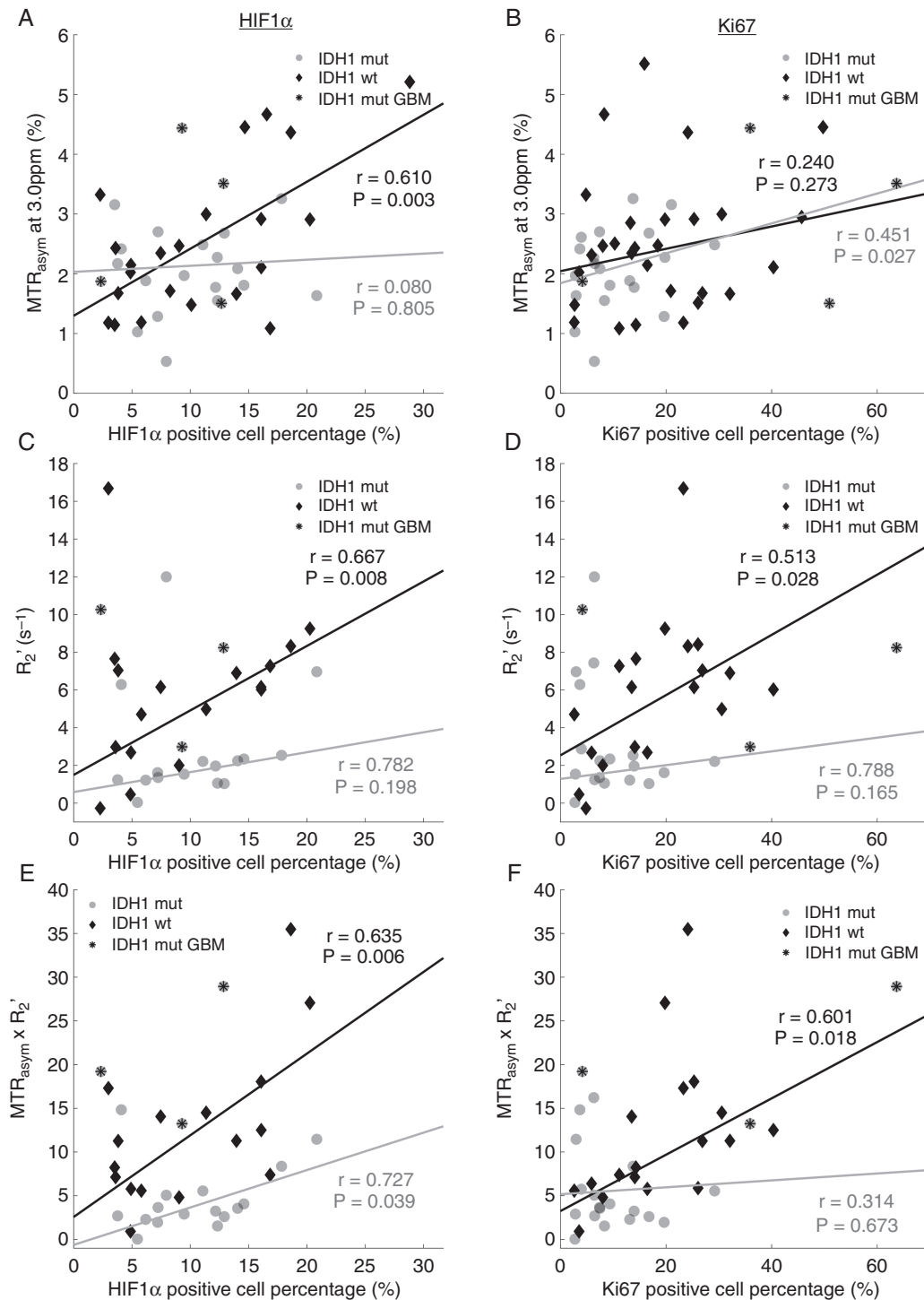
Fig. 6 Association between pH- and hypoxia-weighted MRI features with HIF1α and Ki67 from image-guided biopsies. (A) Correlation between tumor acidity (MTR$_{asym}$ at 3 ppm) and HIF1α expression, (B) MTR$_{asym}$ at 3 ppm and Ki67 expression, (C) hypoxia (R$_2$') and HIF1α expression, (D) R$_2$' and Ki67 expression, (E) MTR$_{asym}$×R$_2$' and HIF1α expression, and (F) MTR$_{asym}$×R$_2$' and Ki67 expression in IDH1 mutant and wild type gliomas.

with IDH1 mutant gliomas as well as 1p/19q-codeleted IDH1 mutant gliomas having lower acidity and hypoxia. Additionally, results from the current study may provide new insight into the mechanisms in which IDH1 mutation

and 2-HG ultimately affect tumor energy metabolism. Despite the early reports that PHD, like the other αKG-dependent enzymes, is competitively inhibited by 2-HG and subsequently increases HIF1α levels,[11,12] results from

the current study appear to support more recent studies showing D-2-HG accumulation activates PHD,[13] leading to decrease in HIF1α levels and lower expression of HIF1α-responsive genes, including many essential for glycolysis.[34] As enhanced glycolysis is a major cause of tumor acidity,[35] suppression of glycolytic pathway related genes would presumably reduce acidity, which is supported by the present observation of lower MTR_{asym} at 3.0 ppm in IDH1 mutant gliomas. In accordance with the present results, the findings of Khurshed et al[36] also suggested that IDH1 wild type gliomas have high expression of glycolysis related genes, as evaluated by The Cancer Genome Atlas metabolic gene expression analysis and in vitro quantification, whereas IDH1 mutant gliomas overexpress oxidative tricarboxylic acid cycle involved genes.

Interestingly, histological results in the current study suggest that measures of R_2', which are thought to be proportional to oxygen extraction fraction, are positively correlated with HIF1α expression, but only in IDH wild type gliomas. This observation appears consistent with results from Koivunen et al[13] showing that IDH1 mutant gliomas have a blunted HIF response to external hypoxia signaling. Although there are few studies examining R_2' in gliomas, it is conceivable that lower R_2' in IDH1 mutant gliomas could be due to lower proliferation rates[37,38] and less angiogenesis[15] compared with IDH1 wild type gliomas. Lower observed acidity and hypoxia in IDH1 mutant gliomas may also partially explain the higher sensitivity to radiotherapy and chemotherapy[39–41] and less aggressive clinical course[42,43] compared with their IDH1 wild type counterparts. We would expect similar imaging characterizations in IDH2 mutant gliomas, due to the similar oncometabolic function of IDH1 mutants and IDH2 mutants, although no conclusion can be drawn within this study because of the small sample size (one IDH2 mutant was identified within the 52 IDH1 wild type gliomas). Further investigation is needed to test this hypothesis.

Several limitations of the present study should be addressed. First, MTR_{asym} may not be the best method for estimating pH sensitivity,[44–46] since it can be confounded by other factors. Similarly, R_2' may also be influenced by additional factors other than oxygen extraction, including blood volume and B_0 inhomogeneities. We are continuing to work on technical development of imaging acquisition and post-processing methods, in order to achieve better image quality, correct for confounding factors, and reduce sensitivity to motion and field inhomogeneity. Additionally, several non-invasive MR-based approaches have been shown to differentiate IDH1 mutant from wild type gliomas, including magnetic resonance spectroscopy–based detection of 2-HG,[47] diffusion[48] and perfusion imaging,[15] and amide proton transfer-weighted CEST imaging.[49,50] Future studies comparing these techniques with the current approach are necessary to understand the association between the various physiologic parameters in IDH1 mutant and wild type gliomas. Despite these potential limitations, the proposed method for simultaneous pH- and oxygen-sensitive MRI contrast in clinically realistic acquisition times appears able to provide unique and valuable information about the tumor microenvironment that complements current anatomic and physiologic MRI techniques.

Conclusion

The current study suggests that simultaneous pH- and oxygen-sensitive amine CEST-SAGE-EPI is a clinically feasible and potentially valuable imaging technique for distinguishing between IDH1 mutant and wild type gliomas as well as 1p/19q codeleted from intact IDH1 mutant gliomas. Results suggest that the IDH1 mutation may be associated with lower acidity and vascular hypoxia, supporting the hypothesis that 2-HG produced by mutation of IDH1 activates PHD, resulting in the degradation of HIF1α, subsequently preventing the metabolic shift from oxidative phosphorylation to glycolysis.

Supplementary Material

Supplementary data are available at *Neuro-Oncology* online.

Keywords

CEST-SAGE-EPI | IDH1 mutant gliomas | HIF1α | pH-weighted MRI | tumor metabolism

patent on this technology (US Patent #15/577,664; International PCT/US2016/034886). *Cloughesy*—Advisory Board—Roche/Genentech, Amgen, Tocagen, NewGen, LPath, Proximagen, Celgene, Vascular Biogenics Ltd, Insys, Agios, Cortice Bioscience, Pfizer, Human Longevity, BMS, Merck, Notable Lab, MedQIA.

Authorship statement. Study design: BME, TFC, LML, JY, DAN. Image and data analysis: JY, AC, BME, CR, WHY, SM, DAN, NS, AL, PLN, RMP, WBP, RGE. Manuscript writing and editing: All authors. All authors read and approved the final manuscript.

References

1. Yan H, Parsons DW, Jin G, et al. IDH1 and IDH2 mutations in gliomas. *N Engl J Med.* 2009;360(8):765–773.

2. Ohgaki H, Kleihues P. The definition of primary and secondary glioblastoma. *Clin Cancer Res.* 2013;19(4):764–772.

3. Carrillo JA, Lai A, Nghiemphu PL, et al. Relationship between tumor enhancement, edema, IDH1 mutational status, MGMT promoter methylation, and survival in glioblastoma. *AJNR Am J Neuroradiol.* 2012;33(7):1349–1355.

4. Lai A, Kharbanda S, Pope WB, et al. Evidence for sequenced molecular evolution of IDH1 mutant glioblastoma from a distinct cell of origin. *J Clin Oncol.* 2011;29(34):4482–4490.

5. Ellingson BM, Lai A, Harris RJ, et al. Probabilistic radiographic atlas of glioblastoma phenotypes. *AJNR Am J Neuroradiol.* 2013;34(3):533–540.

6. Chen JR, Yao Y, Xu HZ, Qin ZY. Isocitrate dehydrogenase (IDH)1/2 mutations as prognostic markers in patients with glioblastomas. *Medicine (Baltimore).* 2016;95(9):e2583.

7. Waitkus MS, Diplas BH, Yan H. Isocitrate dehydrogenase mutations in gliomas. *Neuro Oncol.* 2016;18(1):16–26.

8. Dang L, White DW, Gross S, et al. Cancer-associated IDH1 mutations produce 2-hydroxyglutarate. *Nature.* 2009;462(7274):739–744.

9. Masoud GN, Li W. HIF-1α pathway: role, regulation and intervention for cancer therapy. *Acta Pharm Sin B.* 2015;5(5):378–389.

10. Li Z, Bao S, Wu Q, et al. Hypoxia-inducible factors regulate tumorigenic capacity of glioma stem cells. *Cancer Cell.* 2009;15(6):501–513.

11. Xu W, Yang H, Liu Y, et al. Oncometabolite 2-hydroxyglutarate is a competitive inhibitor of α-ketoglutarate-dependent dioxygenases. *Cancer Cell.* 2011;19(1):17–30.

12. Zhao S, Lin Y, Xu W, et al. Glioma-derived mutations in IDH1 dominantly inhibit IDH1 catalytic activity and induce HIF-1alpha. *Science.* 2009;324(5924):261–265.

13. Koivunen P, Lee S, Duncan CG, et al. Transformation by the (R)-enantiomer of 2-hydroxyglutarate linked to EGLN activation. *Nature.* 2012;483(7390):484–488.

14. Parker SJ, Metallo CM. Metabolic consequences of oncogenic IDH mutations. *Pharmacol Ther.* 2015;152:54–62.

15. Kickingereder P, Sahm F, Radbruch A, et al. IDH mutation status is associated with a distinct hypoxia/angiogenesis transcriptome signature which is non-invasively predictable with rCBV imaging in human glioma. *Sci Rep.* 2015;5:16238.

16. Grassian AR, Parker SJ, Davidson SM, et al. IDH1 mutations alter citric acid cycle metabolism and increase dependence on oxidative mitochondrial metabolism. *Cancer Res.* 2014;74(12):3317–3331.

17. Harris RJ, Yao J, Chakhoyan A, et al. Simultaneous pH-sensitive and oxygen-sensitive MRI of human gliomas at 3 T using multi-echo amine proton chemical exchange saturation transfer spin-and-gradient echo echo-planar imaging (CEST-SAGE-EPI). *Magn Reson Med.* 2018;80(5):1962–1978.

18. Sun PZ, Benner T, Copen WA, Sorensen AG. Early experience of translating pH-weighted MRI to image human subjects at 3 Tesla. *Stroke.* 2010;41(10 Suppl):S147–S151.

19. Souba WW. Glutamine and cancer. *Ann Surg.* 1993;218(6):715–728.

20. Kovacević Z, Morris HP. The role of glutamine in the oxidative metabolism of malignant cells. *Cancer Res.* 1972;32(2):326–333.

21. Medina MA, Sánchez-Jiménez F, Márquez J, Rodríguez Quesada A, Núñez de Castro I. Relevance of glutamine metabolism to tumor cell growth. *Mol Cell Biochem.* 1992;113(1):1–15.

22. Harris RJ, Cloughesy TF, Liau LM, et al. pH-weighted molecular imaging of gliomas using amine chemical exchange saturation transfer MRI. *Neuro Oncol.* 2015;17(11):1514–1524.

23. Harris RJ, Cloughesy TF, Liau LM, et al. Simulation, phantom validation, and clinical evaluation of fast pH-weighted molecular imaging using amine chemical exchange saturation transfer echo planar imaging (CEST-EPI) in glioma at 3 T. *NMR Biomed.* 2016;29(11):1563–1576.

24. Geisler BS, Brandhoff F, Fiehler J, et al. Blood-oxygen-level-dependent MRI allows metabolic description of tissue at risk in acute stroke patients. *Stroke.* 2006;37(7):1778–1784.

25. Zhang J, Chen YM, Zhang YT. Blood-oxygenation-level-dependent-(BOLD-) based R2′ MRI study in monkey model of reversible middle cerebral artery occlusion [published online ahead of print February 6, 2011]. *J Biomed Biotechnol.* 2011;2011:318346. doi:10.1155/2011/318346.

26. Jensen-Kondering U, Manavaki R, Ejaz S, et al. Brain hypoxia mapping in acute stroke: back-to-back T2′ MR versus 18F-fluoromisonidazole PET in rodents. *Int J Stroke.* 2017;12(7):752–760.

27. Tóth V, Förschler A, Hirsch NM, et al. MR-based hypoxia measures in human glioma. *J Neurooncol.* 2013;115(2):197–207.

28. Hirsch NM, Toth V, Förschler A, Kooijman H, Zimmer C, Preibisch C. Technical considerations on the validity of blood oxygenation level-dependent-based MR assessment of vascular deoxygenation. *NMR Biomed.* 2014;27(7):853–862.

29. Hatanpaa KJ, Burger PC, Eshleman JR, Murphy KM, Berg KD. Molecular diagnosis of oligodendroglioma in paraffin sections. *Lab Invest.* 2003;83(3):419–428.

30. Ellingson BM, Bendszus M, Boxerman J, et al; Jumpstarting Brain Tumor Drug Development Coalition Imaging Standardization Steering Committee. Consensus recommendations for a standardized brain tumor imaging protocol in clinical trials. *Neuro Oncol.* 2015;17(9):1188–1198.

31. Yao J, Ruan D, Raymond C, et al. Improving B0 correction for pH-weighted amine proton chemical exchange saturation transfer (CEST) imaging by use of k-means clustering and Lorentzian estimation. *Tomography.* 2018;4(3):123–137.

32. Bankhead P, Loughrey MB, Fernández JA, et al. QuPath: open source software for digital pathology image analysis. *Sci Rep.* 2017;7(1):16878.

33. Ellingson BM, Kim HJ, Woodworth DC, et al. Recurrent glioblastoma treated with bevacizumab: contrast-enhanced T1-weighted subtraction maps improve tumor delineation and aid prediction of survival in a multicenter clinical trial. *Radiology.* 2014;271(1):200–210.

34. Chesnelong C, Chaumeil MM, Blough MD, et al. Lactate dehydrogenase A silencing in IDH mutant gliomas. *Neuro Oncol.* 2014;16(5):686–695.

35. Chiche J, Brahimi-Horn MC, Pouysségur J. Tumour hypoxia induces a metabolic shift causing acidosis: a common feature in cancer. *J Cell Mol Med.* 2010;14(4):771–794.

36. Khurshed M, Molenaar RJ, Lenting K, Leenders WP, van Noorden CJF. In silico gene expression analysis reveals glycolysis and acetate anaplerosis in IDH1 wild-type glioma and lactate and glutamate anaplerosis in IDH1-mutated glioma. *Oncotarget.* 2017;8(30):49165–49177.

37. Zeng A, Hu Q, Liu Y, et al. IDH1/2 mutation status combined with Ki-67 labeling index defines distinct prognostic groups in glioma. *Oncotarget.* 2015;6(30):30232–30238.

38. Bralten LB, Kloosterhof NK, Balvers R, et al. IDH1 R132H decreases proliferation of glioma cell lines in vitro and in vivo. *Ann Neurol.* 2011;69(3):455–463.

39. Cairncross JG, Wang M, Jenkins RB, et al. Benefit from procarbazine, lomustine, and vincristine in oligodendroglial tumors is associated with mutation of IDH. *J Clin Oncol.* 2014;32(8):783–790.

40. Shi J, Sun B, Shi W, et al. Decreasing GSH and increasing ROS in chemosensitivity gliomas with IDH1 mutation. *Tumour Biol.* 2015;36(2):655–662.

41. Tran AN, Lai A, Li S, et al. Increased sensitivity to radiochemotherapy in IDH1 mutant glioblastoma as demonstrated by serial quantitative MR volumetry. *Neuro Oncol.* 2014;16(3):414–420.

42. Houillier C, Wang X, Kaloshi G, et al. IDH1 or IDH2 mutations predict longer survival and response to temozolomide in low-grade gliomas. *Neurology.* 2010;75(17):1560–1566.

43. Parsons DW, Jones S, Zhang X, et al. An integrated genomic analysis of human glioblastoma multiforme. *Science.* 2008;321(5897):1807–1812.

44. Rerich E, Zaiss M, Korzowski A, Ladd ME, Bachert P. Relaxation-compensated CEST-MRI at 7 T for mapping of creatine content and pH–preliminary application in human muscle tissue in vivo. *NMR Biomed.* 2015;28(11):1402–1412.

45. Zaiss M, Xu J, Goerke S, et al. Inverse Z-spectrum analysis for spillover-, MT-, and T1 -corrected steady-state pulsed CEST-MRI–application to pH-weighted MRI of acute stroke. *NMR Biomed.* 2014;27(3):240–252.

46. Xu J, Zaiss M, Zu Z, et al. On the origins of chemical exchange saturation transfer (CEST) contrast in tumors at 9.4 T. *NMR Biomed.* 2014;27(4):406–416.

47. Leather T, Jenkinson MD, Das K, Poptani H. Magnetic resonance spectroscopy for detection of 2-hydroxyglutarate as a biomarker for IDH mutation in gliomas. *Metabolites.* 2017;7(2). doi:10.3390/metabo7020029.

48. Lee S, Choi SH, Ryoo I, et al. Evaluation of the microenvironmental heterogeneity in high-grade gliomas with IDH1/2 gene mutation using histogram analysis of diffusion-weighted imaging and dynamic-susceptibility contrast perfusion imaging. *J Neurooncol.* 2015;121(1):141–150.

49. Jiang S, Zou T, Eberhart CG, et al. Predicting IDH mutation status in grade II gliomas using amide proton transfer-weighted (APTw) MRI. *Magn Reson Med.* 2017;78(3):1100–1109.

50. Paech D, Windschuh J, Oberhollenzer J, et al. Assessing the predictability of IDH mutation and MGMT methylation status in glioma patients using relaxation-compensated multipool CEST MRI at 7.0 T. *Neuro Oncol.* 2018;20(12):1661–1671.